Geophysical Research Letters

RESEARCH LETTER
10.1029/2021GL095836

Key Points:

- Temperature-humidity ($\theta - q$) similarity varies with Bowen ratio (β) in the convective boundary layer (CBL) over homogeneous surface
- $\theta - q$ dissimilarity with varying β is mostly linked to the large-scale eddies
- Disproportional variations of σ_θ^2 and σ_q^2 by asymmetric top-down and bottom-up transport of θ and q explain the dissimilarity with varying β

Supporting Information:

Supporting Information may be found in the online version of this article.

Correspondence to:

H. Liu,
heping.liu@wsu.edu

Citation:

Liu, C., Liu, H., Huang, J., & Xiao, H. (2021). Varying partitioning of surface turbulent fluxes regulates temperature-humidity dissimilarity in the convective atmospheric boundary layer. *Geophysical Research Letters*, *48*, e2021GL095836. https://doi.org/10.1029/2021GL095836

Received 26 AUG 2021
Accepted 24 OCT 2021

Author Contributions:

Conceptualization: Heping Liu
Methodology: Cheng Liu
Project Administration: Hongwei Xiao
Resources: Hongwei Xiao
Software: Cheng Liu, Jianping Huang
Supervision: Heping Liu, Jianping Huang
Visualization: Cheng Liu
Writing – original draft: Cheng Liu
Writing – review & editing: Heping Liu, Jianping Huang

Varying Partitioning of Surface Turbulent Fluxes Regulates Temperature-Humidity Dissimilarity in the Convective Atmospheric Boundary Layer

Cheng Liu[1], Heping Liu[2], Jianping Huang[3,4], and Hongwei Xiao[1]

[1]Jiangxi Province Key Laboratory of the Causes and Control of Atmospheric Pollution/School of Water Resources and Environmental Engineering, East China University of Technology, Nanchang, China, [2]Department of Civil and Environmental Engineering, Washington State University, Pullman, WA, USA, [3]Environmental Modeling Center, NOAA National Centers for Environmental Prediction, I.M. System Group, College Park, MD, USA, [4]Center for Spatial Information Science and Systems, College of Science, George Mason University, Fairfax, VA, USA

Abstract Experimental evidence shows that temperature-humidity ($\theta - q$) similarity in the atmospheric surface layer (ASL) is reduced as Bowen ratio (β) increases over land. However, underlying physical mechanisms remain not well understood. With large-eddy simulations, $\theta - q$ dissimilarity is investigated in the steady-state, convective boundary layer (CBL) over homogeneous landscape with varying β. As β increases from 0.4 to 2.0, the entrainment ratio for θ slightly decreases but that for q largely increases. As a result, local production of humidity variance is substantially enhanced in the upper CBL and transported to the lower CBL by vigorous large eddies, contributing significantly to nonlocal fraction. However, the increased temperature variance in the ASL associated with strong heat flux is larger than that transported from the upper CBL. Such asymmetry in vertical diffusion induced by varying partitioning of surface fluxes strongly regulates $\theta - q$ dissimilarity even under perfect conditions valid for Monin-Obukhov similarity theory.

Plain Language Summary The behavior of potential temperature (θ) and specific humidity (q) in the atmospheric surface layer (ASL) is assumed to be similar over homogeneous landscape. However, abundant experimental evidence shows that such assumption of $\theta - q$ similarity is not satisfied as evaporation decreases (i.e., increased Bowen ratio, β). In order to understand the intrinsic physical mechanism, we investigate $\theta - q$ similarity in the steady-state convective boundary layer (CBL) using the high-resolution model and analyze the results in various β cases. We confirm that $\theta - q$ similarity is reduced across the CBL with increasing or decreasing β from 0.4, with the lowest similarity appearing in the middle or upper CBL. The disproportional variations of σ_θ^2 and σ_q^2 associated with asymmetric contributions by top-down and bottom-up transport of θ and q under varying β conditions explain the $\theta - q$ dissimilarity in the CBL. The results suggest that varying degrees of validity of similarity assumption with changes in β should be noted in applying Monin-Obukhov similarity theory and interpreting eddy covariance data even over homogenous landscapes and highlight the influence of the CBL processes on the ASL turbulence structures.

1. Introduction

Similarity between scalars (e.g., potential temperature θ and specific humidity q) is a widely used theoretical approximation not only in field experiments to derive surface fluxes, but also in numerical models to determine turbulent fluxes and transport of heat, water vapor, and other scalars in the atmospheric surface layer (ASL) (Asanuma et al., 2007; Cancelli et al., 2014; Foken, 2006). The similarity of two scalars implies the equality of their corresponding dimensionless Monin-Obukhov similarity functions (Dias & Brutsaert, 1996), which can be evaluated in various ways, such as eddy diffusivities, similarity functions, and correlation coefficients (e.g., Cancelli et al., 2012; De Bruin et al., 1993; Katul et al., 2008). Here and throughout, $\theta - q$ similarity is defined as the unity of their correlation coefficient (i.e., $R_{\theta q} = 1$) (Hill, 1989), whereas dissimilarity means that $R_{\theta q}$ is less than 1. However, field measurements indicate that the dissimilarity between θ and q is almost always observed under different Bowen ratios (β, a ratio of surface-sensible heat flux to latent heat flux), though the dissimilarity degree varies distinctly across field sites and

experimental conditions (e.g., De Bruin et al., 1993; Dias & Brutsaert, 1996; Katul et al., 2008; Li & Bou-Zeid, 2011; Moene & Schüttemeyer, 2008). Even under steady-state and homogeneous conditions to satisfy the assumptions required by the Monin-Obukhov similarity theory (MOST), dissimilarity is often reported (Cancelli et al., 2014). The presence of such $\theta - q$ dissimilarity poses large challenges to many applications of MOST such as flux-variance and energy-budget Bowen ratio methods and many numerical models in determining turbulent fluxes (Dias & Brutsaert, 1996; Gao et al., 2018). Improving our understanding of the underlying physical mechanisms for $\theta - q$ dissimilarity under different β conditions remains a subject of active research.

Previous studies have suggested that $\theta - q$ dissimilarity is caused by several possible factors such as unsteadiness of turbulence flows (McNaughton & Laubach, 1998), local advection (Lee et al., 2004), surface heterogeneity (Detto et al., 2008; Huang et al., 2009; Moene & Schüttemeyer, 2008; Moene et al., 2006; Williams et al., 2007), different active-passive roles of the scalars (Katul & Parlange, 1994), and entrainment at the top of the atmospheric boundary layer (ABL) (Babić et al., 2021; Boer et al., 2014; Cancelli et al., 2014; De Bruin et al., 1993; Detto et al., 2008; Gao et al., 2018; Katul et al., 2008; Lohou et al., 2010). It is reported that $\theta - q$ dissimilarity in the ASL results from interactions between the ABL processes (e.g., entrainment induced) and surface forcing. Nevertheless, it is rather difficult to identify specific causes for $\theta - q$ dissimilarity with field experiments alone, given the complexity of multiple processes contributing to the dissimilarity (Cancelli et al., 2014). Therefore, it is critical to examine how varying surface-sensible and latent heat fluxes regulates the ABL processes that impact the ASL $\theta - q$ dissimilarity, which motivates the work here via large-eddy simulations (LESs).

As pointed out by Cancelli et al. (2012), $\theta - q$ dissimilarity in the ASL can be connected to the magnitudes of surface-sensible and latent heat fluxes and the consequent establishment of a balance between gradient production and molecular dissipation of scalar variance and covariance. Cancelli et al. (2014) further deduced that the imbalance is likely attributed to weak surface flux that allows turbulence transport and top-down mixing (entrainment) to play an increased role in regulating the ASL dissimilarity. Such conditions with weak surface flux correspond to cases for humidity over the dry land (i.e., high β) and temperature over water surface (i.e., low β). This argument is supported by eddy-covariance measurements that $\theta - q$ dissimilarity is more prominent under drier surface conditions (i.e., higher β) and humidity variance deviates noticeably from the MOST universal function (e.g., De Bruin et al., 1993; Lamaud & Irvine, 2006; Moene et al., 2006). More recently, Babić et al. (2021) found that $R_{\theta q}$ is larger over the slope with low β than over the valley floor with high β. Varying partitioning of surface-sensible and latent heat fluxes (i.e., changes in β) leads to different entrainment regimes for θ and q, as indicated by different entrainment ratios (ratio of entrainment flux to surface flux) (Boer et al., 2014; Mahrt, 1991; Moene et al., 2006). In a high β situation, turbulence is vigorous, and large eddies produced in the convective boundary layer (CBL) can affect the ASL. The relative influence of large CBL eddies on θ in the ASL is small because the surface-sensible heat flux is dominantly large (i.e., local process dominates), while the impact on q is significant due to the low latent heat flux (De Bruin et al., 1993; Mahrt, 1991). Though these field works support the role of varying β in affecting $\theta - q$ dissimilarity, how the CBL processes respond to changes in β which in turn affect $\theta - q$ dissimilarity across the CBL remains underexplored.

LES has been widely employed to study the ABL-related issues, and the model outputs are usually treated as "true" observation data (e.g., Huang et al., 2011; Moeng, 1984; Sullivan & Patton, 2011). In this study, LES experiments are conducted with prescribed vertical profiles of θ and q and varying β to quantify the $\theta - q$ dissimilarity in the buoyancy-driven CBL under homogeneous surface conditions. With the adoption of idealized periodic lateral boundary conditions and focusing on the quasi steady turbulence flow, the role of varying β in $\theta - q$ dissimilarity can be isolated from other factors such as local advection, nonstationarity, and surface heterogeneity. Therefore, the impact on the $\theta - q$ dissimilarity can be caused only by the CBL turbulence processes induced by the initial conditions and varying β. The study aims to investigate how the varying partitioning of surface turbulent fluxes regulates $\theta - q$ dissimilarity in the CBL, with an emphasis on the physical mechanisms based on variance budget analysis.

2. Model and Methods

2.1. LES Configurations

The LES code employed in this study was originally developed by Moeng (1984) and later refined by Sullivan et al. (1996), Patton et al. (2005), and Huang et al. (2009, 2011). The simulation domain size in this study is set to 5.0 × 5.0 × 1.92 km with a grid spacing of 12.5 × 12.5 × 5 m in the x, y, and z directions, respectively. Such domain size and grid mesh are sufficient to well resolve the CBL turbulence flows (Sullivan & Patton, 2011). For all the simulations, geostrophic wind is set to be zero (i.e., shear-free CBL) and a spatially uniform surface-sensible and latent heat flux is prescribed (Table S1 in Supporting Information S1). Varying β is implemented through partitioning of the available energy ($R_n - G_0$, 450 W m^{-2} used in this study, where R_n is the net radiation and G_0 is the ground heat flux) into surface-sensible and latent heat fluxes. The surface roughness length in the model domain is set to 0.1 m. MOST is used as the bottom boundary condition to calculate the surface Reynolds stress (Sullivan et al., 1994).

Two sets of LES experiments are completed with different initial vertical profiles (Table S1 in Supporting Information S1). In group 1, both θ and q have similar initial profiles. Specifically, θ and q have constant values of 290 K and 5 g kg^{-1} within the mixed layer, vertical gradients of 0.075 K m^{-1} and 0.075 g kg^{-1} m^{-1} in the interfacial layer (i.e., the entrainment zone), and gradients of 0.003 K m^{-1} and 0.003 g kg^{-1} m^{-1} in the free atmosphere, respectively (Figure S1 in Supporting Information S1). This represents the scenario when an elevated humid air mass associated with mesoscale processes is horizontally advected above the CBL. Seven simulations are then completed with different β conditions. The simulations in group 1 with the perfectly correlated initial and boundary conditions for the θ and q are intended to eliminate the effect of entrainment of the warm dry air (i.e., anticorrelated θ and q) from the free atmosphere on similarity in the CBL and examine whether such identical initial and boundary conditions result in a perfect $\theta - q$ similarity over homogeneous landscape with varying β. In group 2, the initial θ vertical profile is set the same as that in group 1, whereas the initial q profile is different from that in group 1, with a constant of 8 g kg^{-1} within the mixed layer, a vertical gradient of −0.075 g kg^{-1} m^{-1} in the entrainment zone, and a vertical gradient of −0.003 g kg^{-1} m^{-1} in the free atmosphere. Another seven simulations are completed with the settings of group 2 (Table S1 in Supporting Information S1). Note that the initial profiles in group 2 are similar to those used by Huang et al. (2009) based on the data collected during the 1994 field campaign of the Boreal Ecosystem-Atmosphere Study (BOREAS) (Barr & Betts, 1997). Given the similar impacts of varying β on $\theta - q$ dissimilarity between two groups, the simulations in group 1 are presented in the main text, and those in group 2 are primarily provided in the Supporting Information S1.

The time step of integration was dynamically determined with a typical value ranging from 0.4 to 0.8 s in this study. The 200-time-step samples of LES data were postprocessed after the turbulence kinetic energy reached a quasi steady state after about 1-hr spin-up (Huang et al., 2008; Liu et al., 2019). Note that we also calculated the results with 5-time-step samples and found the difference between two output frequency cases to be less than 1.2% (see Figure S2 in Supporting Information S1). The results presented here were obtained from the last 1-hr simulation for each case.

2.2. Scalar Similarity

Temperature-humidity similarity in this study is quantified by their correlation coefficient $R_{\theta q}$ as

$$R_{\theta q} = \frac{\overline{\theta' q'}}{\sigma_\theta \sigma_q}, \tag{1}$$

where σ_θ and σ_q are the standard deviations of θ and q, respectively, and $\overline{\theta' q'}$ is $\theta - q$ covariance. $R_{\theta q}$ varies from −1 to 1 and a perfect similarity is defined when $R_{\theta q} = \pm 1$. Meanwhile, the spectral correlation coefficient $R_{\theta q}(k)$ is used to investigate the scale dependence of similarity or dissimilarity, which is expressed as (e.g., Asanuma et al., 2007)

$$R_{\theta q}(k) = \frac{S_{\theta q}(k)}{\sqrt{S_{\theta\theta}(k) S_{qq}(k)}}, \tag{2}$$

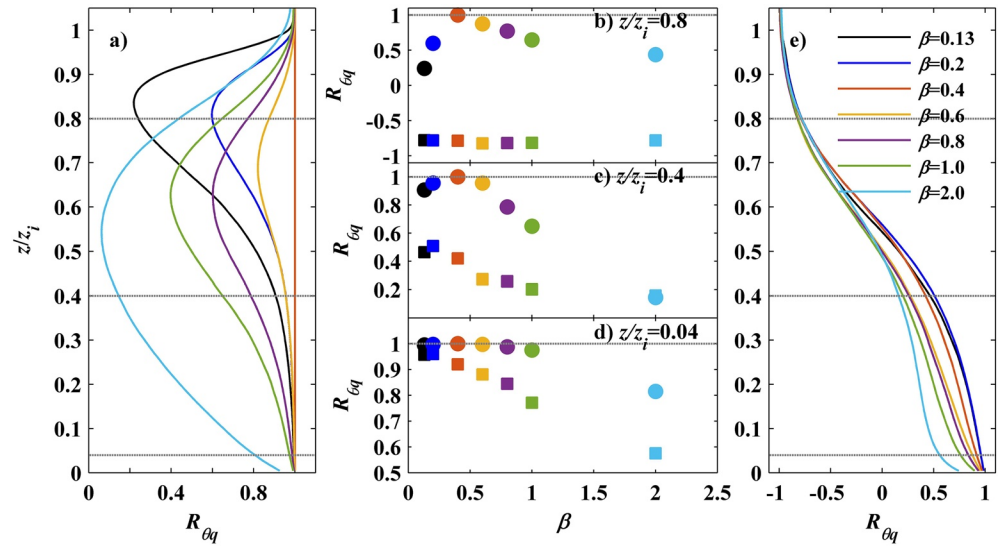

Figure 1. Vertical profiles of correlation coefficient ($R_{\theta q}$) between potential temperature (θ) and specific humidity (q) for group 1 (a) and group 2 (e) at different Bowen ratios (β). $R_{\theta q}$ at $z/z_i = 0.8$, $z/z_i = 0.4$, and $z/z_i = 0.04$ are shown in (b–d), respectively, where circles represent $R_{\theta q}$ for group 1 and squares are for group 2.

where k is the wave number, $S_{\theta\theta}(k)$ and $S_{qq}(k)$ are the spectral density of θ and q, respectively, and $S_{\theta q}(k)$ is the cospectra between θ and q.

3. Results and Discussion

3.1. Changes in $\theta - q$ Dissimilarity With Varying Bowen Ratios

Figure 1 shows vertical profiles of $R_{\theta q}$ for all simulation cases and $R_{\theta q}$ at $z/z_i = 0.04$, 0.4, and 0.8. In group 1, the perfect correlation between θ and q across the CBL is reached (i.e., $R_{\theta q} = 1$) only when $\beta = 0.4$. In the rest of the cases, however, $R_{\theta q}$ is reduced across the CBL (i.e., $R_{\theta q} < 1$) as β increases from 0.4 to 2.0 or decreases from 0.4 to 0.13. $R_{\theta q}$ generally decreases with increasing heights, reaches its minimum around the middle or upper CBL ($0.5 < z/z_i < 0.9$), and then gradually increases to 1 near the top of the CBL (Figure 1a). Focusing on the ASL and taking $z/z_i = 0.04$ as an example, $R_{\theta q}$ is reduced from 1 to 0.81 as β increases from 0.4 to 2.0 (Figure 1d). Around the middle of the CBL, $R_{\theta q}$ is reduced from 1 at $\beta = 0.4$ to 0.15 at $\beta = 2.0$ and is reduced from 1 to 0.91 as β decreases from 0.4 to 0.13 (Figure 1c). $R_{\theta q}$ shows a similar trend with varying β in the upper CBL (Figure 1b). As shown in Figure 2, the dissimilarity is also evidenced in the horizontal (x-y) distributions of θ and q at the lower, middle, and upper CBL. Cellular turbulent organized structures (TOSs) develop in both the θ and q fields in all cases (Figure 2). The TOSs for the θ fields behave similarly to those of the q fields only when $\beta = 0.4$ at all levels, but they show more distinct patterns as β increases. It reflects that θ and q tend to be organized more differently in their spatial variation patterns at higher β primarily due to the enhanced active role of temperature in affecting turbulent flows that become more convective as β increases. Our results indicate that the perfect $\theta - q$ similarity rarely occurs even over the homogeneous landscape for the CBL flows with the identical initial shapes of the θ and q profiles and the persistently perfectly correlated θ and q as the top boundary conditions. Instead, the dissimilarity shows a strong dependence on β.

To further investigate at what scales dissimilarities occur across β conditions, we present the spectral correlation coefficient $R_{\theta q}(k)$ at three different heights for all the simulated cases in group 1 (Figure 3). At the ASL (i.e., $z/z_i = 0.04$), $R_{\theta q}(k)$ remains constant of one at all scales for $\beta = 0.4$, indicating that a perfect $\theta - q$ similarity does occur at all scales. As β> or <0.4, $R_{\theta q}(k)$ at large scales is reduced. As the height increases, $R_{\theta q}(k)$ at large scales is further reduced and even becomes negative for $\beta = 1.0$ and 2.0 at $z/z_i = 0.4$ and $z/z_i = 0.8$ and for $\beta = 0.13$ and $\beta = 0.2$ at $z/z_i = 0.8$. In addition, the scales with dissimilarity are gradually shifted to smaller ones at $z/z_i = 0.4$ and $z/z_i = 0.8$, even though most of the loss in $R_{\theta q}(k)$ still originates

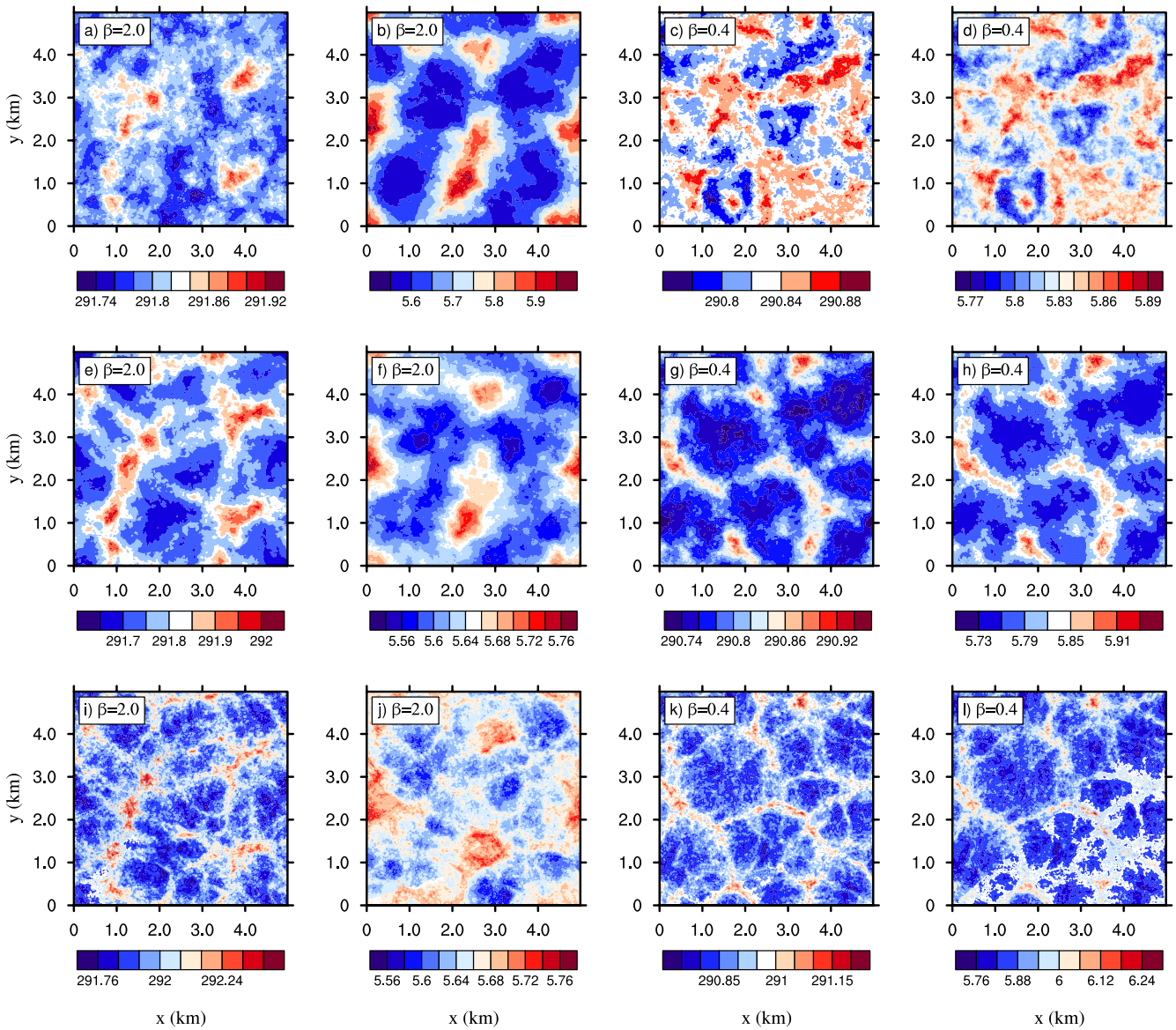

Figure 2. Horizontal (x–y) distributions of θ and q at a height of $z/z_i = 0.8$ (a–d), $z/z_i = 0.4$ (e–h), and $z/z_i = 0.04$ (i–l) for two different β cases ($\beta = 2.0$ and $\beta = 0.4$) in group 1. The first and third columns represent θ fields while the second and fourth columns represent q fields.

from large scales (i.e., $k_x z_i < 4$). Our results indicate that the $\theta - q$ similarity and its variations with varying β observed in Figure 1 are linked to the large-scale eddies that have larger impacts on dissimilarity at higher levels than at lower levels as they progressively penetrate downward. This is supported by the w spectra (Figures 3d–3f), where the $S_{ww}(k)$ difference between various β conditions is more distinct at larger scales than that at smaller scales at higher levels. The x–z cross sections of the θ and q fields in Figure S3 further indicate that top-down eddies (entrainment) lead to more progressive downward invasions of q than θ for higher β cases. Note that the $\theta - q$ dissimilarity with varying β in group 2 is generally consistent with group 1 and is provided in Supporting Information S1.

In summary, our simulations in groups 1 and 2 all indicate that similarity across the CBL is degraded with increasing and decreasing β from 0.4 and is mostly linked to the large-scale eddies.

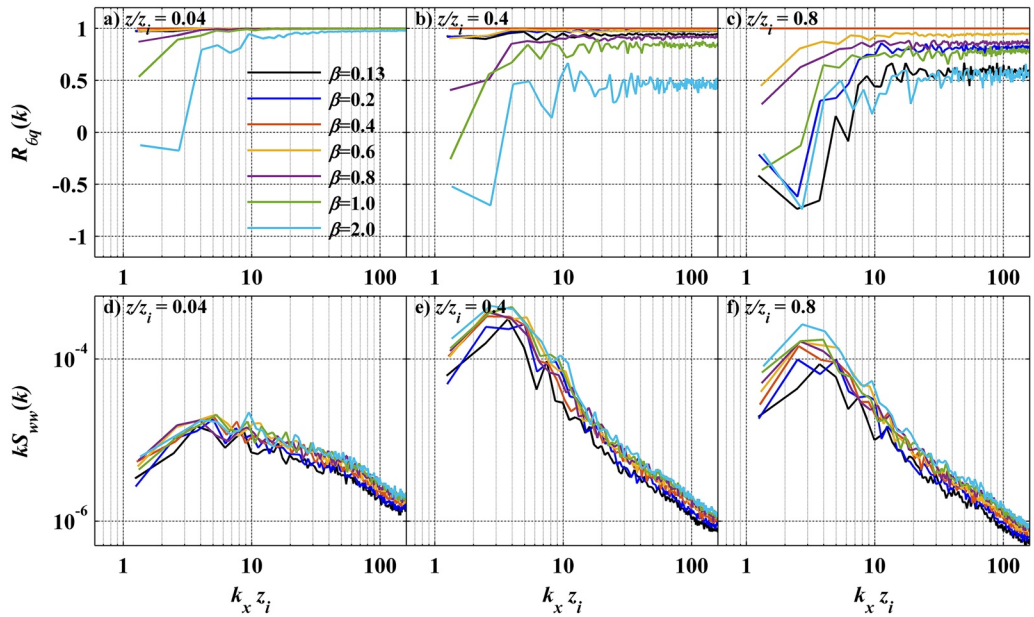

Figure 3. Spectral correlation coefficient ($R_{\theta q}(k)$) between θ and q (top panels) and one-dimensional (x) spectra of the w velocity component ($S_{ww}(k)$) (bottom panels) at the three heights of $z/z_i = 0.04$, 0.4, and 0.8 for group 1.

3.2. Contributions of σ_θ, σ_q and $\overline{\theta' q'}$ and Their Budgets

We now quantify relative contributions of σ_θ, σ_q, and $\overline{\theta' q'}$ to $R_{\theta q}$ with Equation 1. As illustrated in Figures 4a and 4b for group 1, vertical profiles of σ_θ show different variations from those of σ_q as β increases. In other words, σ_θ at all levels of $z/z_i < 1.0$ increases with increasing β, whereas σ_q gradually reduces with increasing β in the lower CBL and then increases with increasing β in the upper CBL. The differences in σ_θ between the $\beta = 0.4$ case and each of the other β cases gradually decrease with heights in the CBL (Figure S5a in Supporting Information S1). However, the differences in σ_q between the $\beta = 0.4$ case and all the $\beta > 0.4$ cases are negative below $z/z_i \approx 0.5$ with the largest magnitudes near the surface, gradually decrease with heights, become positive, and then increase with heights aloft, while the $\beta < 0.4$ cases are just the opposite (Figure S5b in Supporting Information S1). The θ and q spectra show that changes in σ_θ and σ_q with varying β occur at all scales in the lower/middle CBL and primarily at large scales in the upper CBL (Figures S6 and S7). As indicated in Figure 4c, $\overline{\theta' q'}$ is positive throughout the entire CBL, characterized by its reduction across layers as β increases from 0.4 to 2.0 and its decrease from 0.4 to 0.13 below $z/z_i \approx 0.7$ and its significant increase across layers with increasing β above $z/z_i \approx 0.7$. The $\theta - q$ cospectra show that the change in $\overline{\theta' q'}$ with varying β is mainly associated with large-scale processes (Figure S8 in Supporting Information S1). Our calculation indicates that as β increases from 0.4 to 2.0, the increased σ_θ outpaces the decreased σ_q below $z/z_i \approx 0.5$, together with reduced $\overline{\theta' q'}$, and primarily contributes to the reduced $R_{\theta q}$ in the lower CBL (Figures 4a–4c), while the largely increased σ_q and the relatively slightly increased σ_θ along with the increased $\overline{\theta' q'}$ above $z/z_i \approx 0.5$ contribute to the reduced $R_{\theta q}$ in the upper CBL (just the opposite as β decreases from 0.4 to 0.13). The underlying reasons identified to explain the reduced $R_{\theta q}$ with varying β in group 1 remain applicable in explaining the reduced $R_{\theta q}$ in group 2 (see Supporting Information S1).

Physical processes affecting vertical variations in σ_θ and σ_q with varying β are now investigated through the scalar variance budget equation. Under quasistationary and horizontal homogeneous conditions, the budget equation of scalar variance and covariance is given by (Dias & Brutsaert, 1996; Garratt, 1992)

$$\frac{\partial \overline{a'b'}}{\partial t} = 0 = -\overline{w'a'}\frac{\partial \overline{b}}{\partial z} - \overline{w'b'}\frac{\partial \overline{a}}{\partial z} - \frac{\partial \overline{w'a'b'}}{\partial z} - 2\varepsilon_{ab}, \quad (3)$$

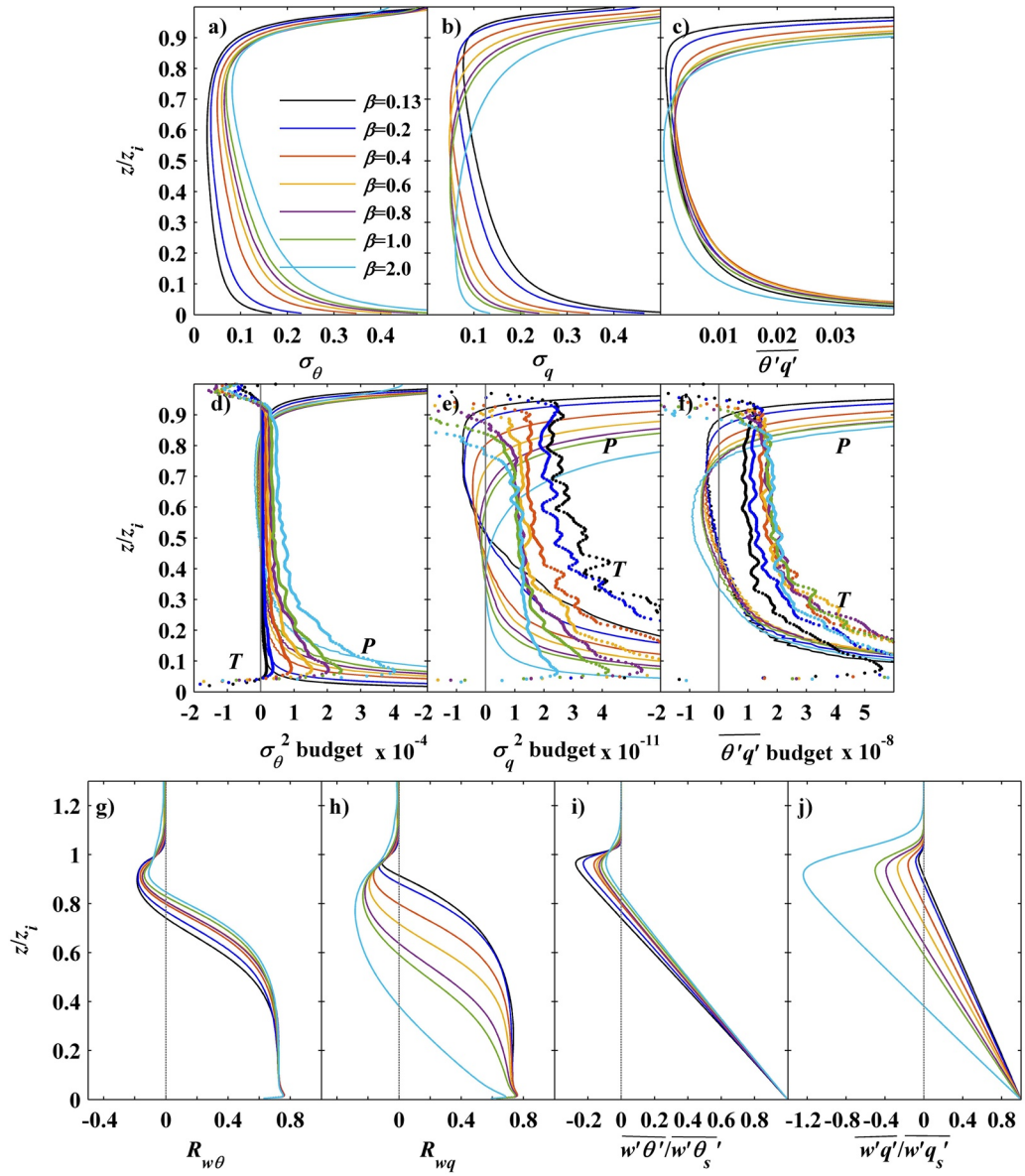

Figure 4. Vertical profiles of (a) standard deviation of θ (σ_θ), (b) standard deviation of q (σ_q), (c) $\theta - q$ covariance ($\overline{\theta' q'}$), and their variance budget (d–f) as well as (g) correlation coefficient between w and θ ($R_{w\theta}$), (h) correlation coefficient between w and q (R_{wq}), (i) heat flux ($\overline{w'\theta'}$), and (j) water vapor flux ($\overline{w'q'}$) for group 1.

where a and b may be either θ or q, and ε_{ab} is the molecular dissipation. The first and the second terms on the right-hand side of Equation 3 represent production terms (P) associated with turbulent flux of scalar and their concentration gradient. The third term is a vertical transport term (T).

The middle panels of Figure 4 show vertical profiles of the production and transport terms in the budget equations for ${\sigma_\theta}^2$, ${\sigma_q}^2$, and $\overline{\theta' q'}$ for group 1. The increased production as a result of enhanced sensible heat flux with increasing β primarily contributes to the enhancement of ${\sigma_\theta}^2$ in the lower CBL, whereas it is insensitive to the increasing β in the upper CBL (Figure 4a vs. 4d). Nonlocal transport by large eddies acts as a dominant source of ${\sigma_\theta}^2$ in the regions of $0.1 < z/z_i < 0.9$, but increases slightly as β increases. It means that as β increases, the increased production leads to the largely increased ${\sigma_\theta}^2$ below $z/z_i \approx 0.2$, while the increased turbulent transport by large eddies results in the increased ${\sigma_\theta}^2$ above $z/z_i \approx 0.2$ (Figure 4a vs. 4d). Different from ${\sigma_\theta}^2$ production, ${\sigma_q}^2$ production is largely reduced below $z/z_i \approx 0.4$–0.5 due to the weakened surface water vapor flux, but enhanced above $z/z_i \approx 0.4$–0.5 because of the enlarged entrainment flux with

increasing β, while its nonlocal turbulent transport by large eddies is consistently reduced within the mixing layer as β increases. Apparently, the change in the ${\sigma_q}^2$ production predominantly regulates σ_q in the lower and upper CBL and the change in the ${\sigma_q}^2$ transport contributes to σ_q within the middle CBL as β increases (Figure 4b vs. 4e). The turbulent transport of $\overline{\theta' q'}$ by large eddies is insensitive to the increased β for all $\beta > 0.4$ cases, and the change in its production mainly regulates the variation of $\overline{\theta' q'}$ in the upper CBL (Figure 4c vs. 4f).

3.3. Physical Mechanisms Causing $\theta - q$ Dissimilarity With Varying β Under Homogeneous Surface

Our results have indicated that $\theta - q$ dissimilarity in the CBL almost always exists under varying β conditions over homogeneous surface even with the perfectly correlated initial and boundary conditions for θ and q in group 1 (Figure 1). TOSs are a primary inherent turbulence feature acting as the most efficient way of transporting heat and water vapor in the CBL (Huang et al., 2009). While TOSs are extensively seen in the spatial distributions of θ and q fields for all the cases, they tend to be organized more differently at higher β (Figure 2), suggesting that TOSs have a distinct transport efficiency in θ and q and play a critical role in regulating dissimilarity. Indeed, there exist differences between heat transport efficiency ($R_{w\theta} = \dfrac{\overline{w'\theta'}}{\sigma_w \sigma_\theta}$) and humidity transport efficiency ($R_{wq} = \dfrac{\overline{w'q'}}{\sigma_w \sigma_q}$) as indicated in Figures 4g and 4h, where $R_{w\theta}$ shows a small change with increasing β across the CBL, but R_{wq} follows a decreasing trend with increasing β in the lower CBL and a largely increasing trend (more negative) in the upper CBL. It indicates that the reduced $\theta - q$ similarity is attributed to the difference of their transport efficiency. Such differences of vertical transport between θ and q are tightly associated with asymmetric variations in bottom-up (surface-flux dominated) and top-down (entrainment-flux dominated) processes for the θ and q as a result of varying partitioning of surface fluxes.

Entrainment ratio $A_s = \overline{w's'}_e / \overline{w's'}_0$ is a useful parameter quantifying the relative importance of the entrainment flux, where s represents scalar (Wyngaard & Brost, 1984). As β increases from 0.13 to 2.0 in group 1, the entrainment ratio for humidity A_q varies from −0.048 to −1.12 (i.e., 2237.5%), which is more significant than that for heat A_θ that changes from −0.273 to −0.092 (i.e., −66.3%) (Table S1 in Supporting Information S1). As a result, entrainment flux has the significantly increased contributions to ${\sigma_q}^2$ and the influence of this increased contributions progressively propagates downward (i.e., top-down effect) as β increases (Figures 4b and 4e), whereas the contributions of entrainment flux to ${\sigma_\theta}^2$ are roughly invariant across β cases (Figures 4a and 4d). As β increases, the effect of bottom-up processes induced by surface-sensible heat flux progressively invades upward into the upper CBL, and the effect induced by surface water vapor flux gradually retreats to lower levels. Therefore, such changes in asymmetric contributions of entrainment fluxes and surface fluxes to θ and q (i.e., asymmetry) with varying β lead to reduced $\theta - q$ similarity. At $\beta = 0.4$, however, A_θ and A_q become identical (Table S1 in Supporting Information S1) and $R_{w\theta}$ is same as R_{wq}, suggesting that the contributions of the top-down entrainment to both ${\sigma_\theta}^2$ and ${\sigma_q}^2$ are comparable to those of the bottom-up transport induced by surface flux (i.e., a symmetry case). As a result, $R_{\theta q}$ approaches one in the CBL with the identical turbulent sources and sinks of heat and humidity in the vertical directions at $\beta = 0.4$. Furthermore, the normalized vertical profiles of $\overline{w'\theta'}$ manifest a slight departure (Figure 4i) but $\overline{w'q'}$ profiles show a large departure as β changes (Figure 4j), highlighting distinct vertical transport of these two turbulent fluxes by large eddies. Note that the free atmosphere provides the background of the CBL growth, the gradient in the entrainment zone plays a direct role in entrainment, and the gradient in the free atmosphere can also influence the gradient in the entrainment zone. Our sensitivity tests show that an increasing $\Delta\theta$ (or a decreasing Δq) slightly enhances the entrainment of θ and largely reduces the entrainment of q, which further modifies the $\theta - q$ dissimilarity (Figure S11 in Supporting Information S1). However, our tests indicate that even though the initial jumps and vertical gradient in the free atmosphere are altered, our conclusions about changes of dissimilarity with varying β remain unchanged (Figure S12 in Supporting Information S1).

4. Conclusions and Implications

Even with steady-state and horizontally homogeneous CBL flows that satisfy the MOST requirements, it is found here that $\theta - q$ similarity across the CBL is largely reduced as a result of varying partitioning of surface turbulent fluxes. The largest $\theta - q$ dissimilarity occurs around the middle or upper CBL. The variance budget analysis indicates that as β increases, the increased σ_θ outpaces the decreased σ_q in the lower CBL, which is more associated with changes in their local productions through the bottom-up turbulent processes. In the upper CBL, however, local production of σ_q is substantially enhanced due to the enlarged entrainment flux and transported to the lower CBL by vigorous large eddies as β increases, while the contributions of entrainment flux to σ_θ are roughly invariant. The disproportional variations of ${\sigma_\theta}^2$ and ${\sigma_q}^2$ associated with asymmetric contributions by top-down and bottom-up transport of θ and q under varying β conditions regulate the $\theta - q$ dissimilarity in the CBL.

Our results suggest that $\theta - q$ similarity is strongly dependent on β. This further reminds us to be cautious when applying MOST-based methods to determine scalar fluxes even under idealized conditions. The results highlight the importance of interactions between the CBL processes and the ASL turbulent exchanges, which in turn lead to changes in the ASL turbulence structures and fluxes (Cheng et al., 2021; Li et al., 2018, 2021; Liu et al., 2021). It should be noted that although other factors (e.g., surface heterogeneity) can also contribute to dissimilarities, the findings in this study can facilitate the understanding of the impact of surface heterogeneity on $\theta - q$ dissimilarity, given that heterogeneous surface consists of patches with different β, which will be investigated in future studies.

Data Availability Statement

Open Research: According to the AGU publications Data Policy, the data used in this paper are deposited in a public repository (https://doi.org/10.5281/zenodo.5070412). Data set citation: Liu, C., Liu, H., Huang, J., & Xiao, H. (2021). Varying partitioning of surface turbulent fluxes regulates temperature-humidity dissimilarity in the convective atmospheric boundary layer [Data set]. Zenodo. http://doi.org/10.5281/zenodo.5070412.

Acknowledgments
The authors wish to thank Dr. Xuelong Chen and the anonymous referees for their constructive comments. C. Liu acknowledges support by the National Natural Science Foundation of China (42105088), the Jiangxi Provincial Natural Science Foundation (20202BAB213019), and the Key Laboratory Project of Jiangxi Province (20171BCD40010). H. Liu acknowledges support by the National Science Foundation (NSF-AGS-1419614 and NSF-AGS-1853050). J. Huang also acknowledges support by the National Natural Science Foundation of China (41575009).

References

Asanuma, J., Tamagawa, I., Ishikawa, H., Ma, Y., Hayashi, T., Qi, Y., & Wang, J. (2007). Spectral similarity between scalars at very low frequencies in the unstable atmospheric surface layer over the Tibetan plateau. *Boundary-Layer Meteorology*, *122*(1), 85–103. https://doi.org/10.1007/s10546-006-9096-y

Babić, N., Stiperski, I., Marinović, I., Večenaj, Ž., & De Wekker, S. F. (2021). Examining relationships between entrainment-driven scalar dissimilarity and surface energy balance underclosure in a semiarid valley. *Agricultural and Forest Meteorology*, *298*, 108272. https://doi.org/10.1016/j.agrformet.2020.108272

Barr, A. G., & Betts, A. K. (1997). Radiosonde boundary layer budgets above a boreal forest. *Journal of Geophysical Research*, *102*(D24), 29205–29212. https://doi.org/10.1029/97JD01105

Boer, A., Moene, A. F., Graf, A., Schüttemeyer, D., & Simmer, C. (2014). Detection of entrainment influences on surface-layer measurements and extension of Monin–Obukhov similarity theory. *Boundary-Layer Meteorology*, *152*(1), 19–44. https://doi.org/10.1007/s10546-014-9920-8

Cancelli, D. M., Chamecki, M., & Dias, N. L. (2014). A large-eddy simulation study of scalar dissimilarity in the convective atmospheric boundary layer. *Journal of the Atmospheric Sciences*, *71*(1), 3–15. https://doi.org/10.1175/JAS-D-13-0113.1

Cancelli, D. M., Dias, N. L., & Chamecki, M. (2012). Dimensionless criteria for the production-dissipation equilibrium of scalar fluctuations and their implications for scalar similarity. *Water Resources Research*, *48*(10), W10522. https://doi.org/10.1029/2012WR012127

Cheng, Y., Li, Q., Li, D., & Gentine, P. (2021). Logarithmic profile of temperature in sheared and unstably stratified atmospheric boundary layers. *Physical Review Fluids*, *6*(3), 034606. https://doi.org/10.1103/PhysRevFluids.6.034606

De Bruin, H. A. R., Kohsiek, W., & Van Den Hurk, B. J. J. M. (1993). A verification of some methods to determine the fluxes of momentum, sensible heat, and water vapour using standard deviation and structure parameter of scalar meteorological quantities. *Boundary-Layer Meteorology*, *63*(3), 231–257. https://doi.org/10.1007/BF00710461

Detto, M., Katul, G., Mancini, M. A. R. C. O., Montaldo, N., & Albertson, J. D. (2008). Surface heterogeneity and its signature in higher-order scalar similarity relationships. *Agricultural and Forest Meteorology*, *148*(6–7), 902–916. https://doi.org/10.1016/j.agrformet.2007.12.008

Dias, N. L., & Brutsaert, W. (1996). Similarity of scalars under stable conditions. *Boundary-Layer Meteorology*, *80*(4), 355–373. https://doi.org/10.1007/BF00119423

Foken, T. (2006). 50 years of the Monin–Obukhov similarity theory. *Boundary-Layer Meteorology*, *119*(3), 431–447. https://doi.org/10.1007/s10546-006-9048-6

Gao, Z., Liu, H., Li, D., Katul, G. G., & Blanken, P. D. (2018). Enhanced temperature-humidity similarity caused by entrainment processes with increased wind shear. *Journal of Geophysical Research: Atmospheres*, *123*(8), 4110–4121. https://doi.org/10.1029/2017JD028195

Garratt, J. R. (1992). *The atmospheric boundary layer* (p. 316). Cambridge University Press.

Hill, R. J. (1989). Implications of Monin–Obukhov similarity theory for scalar quantities. *Journal of the Atmospheric Sciences*, *46*(14), 2236–2244. https://doi.org/10.1175/1520-0469(1989)046<2236:iomstf>2.0.co;2

Huang, J., Lee, X., & Patton, E. G. (2008). A modelling study of flux imbalance and the influence of entrainment in the convective boundary layer. *Boundary-Layer Meteorology*, *127*(2), 273–292. https://doi.org/10.1007/s10546-007-9254-x
Huang, J., Lee, X., & Patton, E. G. (2009). Dissimilarity of scalar transport in the convective boundary layer in inhomogeneous landscapes. *Boundary-Layer Meteorology*, *130*(3), 327–345. https://doi.org/10.1007/s10546-009-9356-8
Huang, J., Lee, X., & Patton, E. G. (2011). Entrainment and budgets of heat, water vapor, and carbon dioxide in a convective boundary layer driven by time-varying forcing. *Journal of Geophysical Research*, *116*, D06308. https://doi.org/10.1029/2010JD014938
Katul, G. G., & Parlange, M. B. (1994). On the active role of temperature in surface-layer turbulence. *Journal of the Atmospheric Sciences*, *51*(15), 21812–2195. https://doi.org/10.1175/1520-0469(1994)051<2181:OTAROT>2.0
Katul, G. G., Sempreviva, A. M., & Cava, D. (2008). The temperature–humidity covariance in the marine surface layer: A one-dimensional analytical model. *Boundary-Layer Meteorology*, *126*(2), 263–278. https://doi.org/10.1007/s10546-007-9236-z
Lamaud, E., & Irvine, M. (2006). Temperature–humidity dissimilarity and heat-to-water-vapour transport efficiency above and within a pine forest canopy: The role of the Bowen ratio. *Boundary-Layer Meteorology*, *120*(1), 87–109. https://doi.org/10.1007/s10546-005-9032-6
Lee, X., Yu, Q., Sun, X., Liu, J., Min, Q., Liu, Y., & Zhang, X. (2004). Micrometeorological fluxes under the influence of regional and local advection: A revisit. *Agricultural and Forest Meteorology*, *122*(1–2), 111–124. https://doi.org/10.1016/j.agrformet.2003.02.001
Li, D., & Bou-Zeid, E. (2011). Coherent structures and the dissimilarity of turbulent transport of momentum and scalars in the unstable atmospheric surface layer. *Boundary-Layer Meteorology*, *140*(2), 243–262. https://doi.org/10.1007/s10546-011-9613-5
Li, Q., Cheng, Y., & Gentine, P. (2021). Connection between mass flux transport and eddy diffusivity in convective atmospheric boundary layers. *Geophysical Research Letters*, *48*(8), e2020GL092073. https://doi.org/10.1029/2020GL092073
Li, Q., Gentine, P., Mellado, J. P., & McColl, K. A. (2018). Implications of nonlocal transport and conditionally averaged statistics on Monin–Obukhov similarity theory and Townsend's attached eddy hypothesis. *Journal of the Atmospheric Sciences*, *75*(10), 3403–3431. https://doi.org/10.1175/JAS-D-17-0301.1
Liu, C., Fedorovich, E., Huang, J., Hu, X. M., Wang, Y., & Lee, X. (2019). Impact of aerosol shortwave radiative heating on entrainment in the atmospheric convective boundary layer: A large-eddy simulation study. *Journal of the Atmospheric Sciences*, *76*(3), 785–799. https://doi.org/10.1175/JAS-D-18-0107.1
Liu, H., Gao, Z., & Katul, G. G. (2021). Non-closure of surface energy balance linked to asymmetric turbulent transport of scalars by large eddies. *Journal of Geophysical Research: Atmospheres*, *126*(7), e2020JD034474. https://doi.org/10.1029/2020JD034474
Lohou, F., Saïd, F., Lothon, M., Durand, P., & Serça, D. (2010). Impact of boundary-layer processes on near-surface turbulence within the West African monsoon. *Boundary-Layer Meteorology*, *136*(1), 1–23. https://doi.org/10.1007/s10546-010-9493-0
Mahrt, L. (1991). Boundary-layer moisture regimes. *Quarterly Journal of the Royal Meteorological Society*, *117*(497), 151–176. https://doi.org/10.1002/qj.49711749708
McNaughton, K. G., & Laubach, J. (1998). Unsteadiness as a cause of non-equality of eddy diffusivities for heat and vapour at the base of an advective inversion. *Boundary-Layer Meteorology*, *88*(3), 479–504. https://doi.org/10.1023/A:1001573521304
Moene, A. F., & Schüttemeyer, D. (2008). The effect of surface heterogeneity on the temperature–humidity correlation and the relative transport efficiency. *Boundary-Layer Meteorology*, *129*(1), 99–113. https://doi.org/10.1007/s10546-008-9312-z
Moene, A. F., Schüttemeyer, D., & Hartogensis, O. K. (2006). Scalar similarity functions: The influence of surface heterogeneity and entrainment. In *17th symposium on boundary layers and turbulence* (p. 1). American Meteorological Society.
Moeng, C. H. (1984). A large-eddy-simulation model for the study of planetary boundary-layer turbulence. *Journal of the Atmospheric Sciences*, *41*(13), 20522–2062. https://doi.org/10.1175/1520-0469(1984)041<2052:alesmf>2.0.co;2
Patton, E. G., Sullivan, P. P., & Moeng, C. H. (2005). The influence of idealized heterogeneity on wet and dry planetary boundary layers coupled to the land surface. *Journal of the Atmospheric Sciences*, *62*(7), 2078–2097. https://doi.org/10.1175/JAS3465.1
Sullivan, P. P., McWilliams, J. C., & Moeng, C. H. (1994). A subgrid-scale model for large-eddy simulation of planetary boundary-layer flows. *Boundary-Layer Meteorology*, *71*(3), 247–276. https://doi.org/10.1007/BF00713741
Sullivan, P. P., McWilliams, J. C., & Moeng, C. H. (1996). A grid nesting method for large-eddy simulation of planetary boundary-layer flows. *Boundary-Layer Meteorology*, *80*(1), 167–202. https://doi.org/10.1007/BF00119016
Sullivan, P. P., & Patton, E. G. (2011). The effect of mesh resolution on convective boundary layer statistics and structures generated by large-eddy simulation. *Journal of the Atmospheric Sciences*, *68*(10), 2395–2415. https://doi.org/10.1175/JAS-D-10-05010.1
Williams, C. A., Scanlon, T. M., & Albertson, J. D. (2007). Influence of surface heterogeneity on scalar dissimilarity in the roughness sublayer. *Boundary-Layer Meteorology*, *122*(1), 149–165. https://doi.org/10.1007/s10546-006-9097-x
Wyngaard, J. C., & Brost, R. A. (1984). Top-down and bottom-up diffusion of a scalar in the convective boundary layer. *Journal of the Atmospheric Sciences*, *41*(1), 102–112. https://doi.org/10.1175/1520-0469(1984)041<0102:TDABUD>2.0

References From the Supporting Information

Chen, X., Anel, J. A., Su, Z., de la Torre, L., Kelder, H., van Peet, J., & Ma, Y. (2013). The deep atmospheric boundary layer and its significance to the stratosphere and troposphere exchange over the Tibetan Plateau. *PLoS One*, *8*(2), e56909. https://doi.org/10.1371/journal.pone.0056909
Stull, R. B. (1988). *An introduction to boundary layer meteorology* (p. 666). Kluwer Academic Publishers.